Examination of Thermoelectric Power of the $CuInGaSe_2$ Crystals

A. Salem[a,*], K. Alshehri[b],
J.A. Mohammed Abdulwahed[c] and S.A. Hussein[a]

[a] *Solid Sate Lab., Physics Department, Faculty of Science, South Valley University, Qena, Egypt*
[b] *Physics Department, University of Bisha, Saudi Arabia*
[c] *Physics Department, Umm Al-Qura University College in Qunfudah – Female, KSA*

Received: 10.01.2022 & Accepted: 18.05.2022

Doi: 10.12693/APhysPolA.142.211 *e-mail: drabouelwafasalem@gmail.com

Within the temperature range 186–424 K, the rate of change in the thermoelectric power as a function of temperature of the $CuInGaSe_2$ compound is measured. The $CuInGaSe_2$ compound was crystallised using a modified Bridgman process. According to measurements, the crystals' conductivity was p-type. The relationship between thermoelectric power, charge carrier concentration, and electrical conductivity was investigated. Several physical characteristics, including mobilities, diffusion coefficients, diffusion lengths, effective masses, and carrier relaxation times, were determined using the experimental data. These characteristics reveal the semiconductor's overall behaviour. Our results show that as-grown $CuInGaSe_2$ crystals are generally p-type and can be potential candidates for thermoelectric power generation.

topics: $CuInGaSe_2$ (CIGS), crystals, characterization of semiconducting quaternary compounds

1. Introduction

The principle of directly converting heat to electricity is not new. Thomas Seebeck, a German physicist, discovered it in 1822. He found that when two different conductive materials (iron and copper) are coupled in a closed circuit, and two contacts are held at different temperatures, an electric voltage is formed. When the two contacts are thermoelectrically connected, a phenomenon known as the Seebeck effect develops.

In recent years, growing concern about environmental issues such as emissions, and particularly global warming and energy resource scarcity, has resulted in substantial research into novel electrical power generation methods [1]. Due to their unique characteristics, thermoelectric generators have become a viable alternative to green technology. Without considering the cost of thermal energy intake, thermoelectric power generation has possible applications in directly converting waste heat energy to electrical power. The efficiency of the total energy conversion system is improved by using this alternative green technology to directly transform waste-heat energy into electrical energy [2].

Semiconductors have a variety of beneficial features that can be applied to a wide range of high-performance devices in sectors such as electronics and optoelectronics. Because of its multiple advantages, the I–III–VI_2 family of semiconducting compounds, which includes $CuIn_{1-x}Ga_xSe_2$ (CIGS), has been widely used in photovoltaics. Copper indium gallium diselenide (CIGS) may be of interest for solar cell applications. In recent years, photovoltaic power generation technology based on $Cu(In,Ga)Se_2$ has been greatly improved [3–6]. Over 23% efficiency in power conversion has been achieved [7, 8] due to the polycrystalline nature of the absorber. The fundamental issues of CIGS technology in terms of absorber layer characteristics and system design for next-generation solar cells have already been recognized [9]. Because of its high light absorption and tunable bandgap, $Cu(In,Ga)Se_2$ (CIGS) is the best material option for solar cells, though future performance enhancements will have to rely on nanostructures, which have received a lot of attention in recent years [10]. As a result of the investigation into the thermoelectric power of $CuInGaSe_2$ crystals, this paper gives detailed data on the basic physical characteristics. This study provides, exacts, and directs data on mobilities, diffusion coefficients, diffusion lengths, effective masses, and carrier relaxation durations.

2. Experimental

In the solid-state laboratory, $CuInGaSe_2$ crystals were produced from a melt using the Bridgman process. For crystal formation, a unique design was adopted. This design shows that the driving

force necessary to move a filled silica ampoule is equal to the drop in the water level in a particular container, which indicates the velocity of motion. The design philosophy, as well as the procedure details, were previously disclosed [11]. The samples obtained were high-quality crystals that were brittle and had a layer structure. The X-ray diffraction technique was used to check the crystal perfection. The index data of the American Society for Testing Materials (ASTM) cards were compared to the diffraction for these materials. According to these X-ray measurements, the crystals show a high degree of crystallinity, indicating that the preparation procedure is sufficiently reliable and satisfactory.

The sample was prepared in the required size of 12.5 mm in diameter and 3.2 mm in thickness, supported vertically by two holders, with the lower one acting as a heat source and the other as a heat sink, and then placed within a high vacuum tight calorimeter developed specifically for this purpose [12]. A thin film of mica separated the sample from the holders. For thermoelectric power (TEP) measurements, an evacuated working chamber (10^{-3} Torr) was locally constructed and designed to protect the samples from oxidation and condensation of water vapour at high and low temperatures, respectively. The outer heater discharges its heat slowly into the specimen environment. The internal heater is placed at the lower end of the crystal to control the temperature of the entire sample and its gradient, which allows measurement in a wide temperature range. The average of the temperatures at the crystal's two ends was used to determine its temperature. Simultaneous temperature and potential deference measurements were taken in an attempt to improve accuracy. In this work, a compensating method was employed to measure voltage without consuming significant current using a tight potentiometer (UJ33E). We needed the temperature to be distributed uniformly, so we placed silver paste across the ends of the object in a uniform pattern. A two-part holder was utilised to make the temperature difference along the crystal in a direction perpendicular to the natural cleavage plane. More details about the apparatus and technique of measuring have been published [12, 13]. The experiments were carried out under a vacuum to eliminate the effects of water vapour condensation in the low-temperature range and oxidation in the high-temperature range. Measurements were taken at a variety of temperatures ranging from 186 to 424 K during this experiment.

3. Results and discussion

The microstructure of the materials has a big impact on their thermoelectric properties. The Fermi level, which is dependent on the carrier concentration, carrier effective mass, and temperature, substantially influences the Seebeck coefficient [14], whereas electronic and morphological defects might limit electrical conductivity [15]. The Seebeck coefficient was improved by distorting the electronic density of states and principals to double the power factor, and it was further clarified that in nanostructure materials, it could provide us with better-quality outcomes [16]. Figure 1a shows the fluctuation of the $CuInGaSe_2$ crystal's differential thermoelectric power as a function of temperature. The following points are highlighted:

- Within the temperature range of examination, our sample exhibits p-type conductivity, which is consistent with our earlier Hall coefficient results [17].
- The TEP value for $CuInGaSe_2$ mounted at 39.66 μV/K at room temperature.
- The TEP value rises until it reaches its maximum value of 99 μV/K, which corresponds to $T = 254$ K. As a result of this behaviour, it was assumed that more holes were created, which contributed to the increase of the α values as the temperature went up. The value of the thermoelectric power drops as the temperature rises, until it reaches a low value of 1.2 μV/K at 329 K, as seen in Fig. 1a. This may be due to the presence of some crystal defects or trapping centers in the direction of the carrier flow.
- In Fig. 1a, there is a third zone where α rapidly falls above 340 K.
- As the temperature rises, the rate of TEP increases. Such behaviour is predicted in this intrinsic range, where both carriers (electrons and holes) contribute to the increase in α value. The discussion on the outcome can be split into two parts, namely, the intrinsic and extrinsic regions.

As a result, we can estimate a wide range of physical properties, including the TEP of a semiconductor. In the intrinsic area, this quantity can be expressed as follows [18]

$$\alpha = \frac{k_{\mathrm{B}}}{e}\left[\frac{b-1}{b+1}\left(\frac{\Delta E_g}{2k_{\mathrm{B}}T}+2\right)+\frac{1}{2}\ln\left(\left(\frac{m_n^*}{m_p^*}\right)^{\frac{3}{2}}\right)\right], \tag{1}$$

where b is the ratio between the mobility of electrons and holes, k_{B} is the Boltzmann constant, m_n^* and m_p^* are the effective masses of electrons and holes, respectively, and ΔE_g is the width of the forbidden energy band. The electrical conductivity σ in Fig. 1b increases as the temperature rises, indicating the semiconductor characteristics. The thermal energy excites free electrons from the valence band to the conduction band as the temperature rises, resulting in greater electrical conductivity.

The dependency of α as a function of the reciprocal of the temperature inside the intrinsic range turns out to be a line, as shown in Fig. 2. The carrier effective masses and the electron to hole mobility ratio are calculated using the measured thermoelectric power and value of ΔE_g. The slopes of

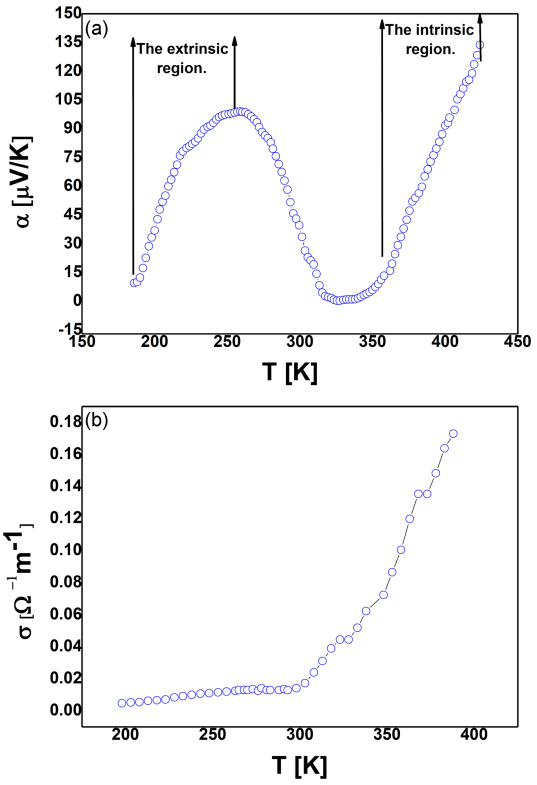

Fig. 1. Temperature dependence of the studied samples' Seebeck coefficient α (a) and electrical conductivity σ (b) for the investigated $CuInGaSe_2$ crystal.

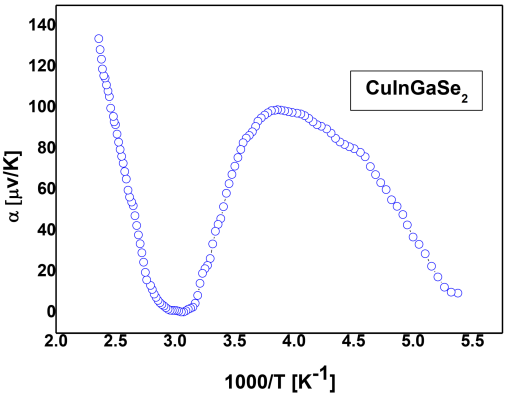

Fig. 2. Temperature reliance of the thermoelectric power α plotted vs inverse temperature $(1000/T)$ for the investigated $CuInGaSe_2$ crystal.

the curves of the thermoelectric power α vs $1/T$, and therefore the intercepts of the curves, are used to calculate $b = \mu_n/\mu_p = 3.23$. We can calculate $\mu_n = 25.22 \times 10^{-4}$ m^2/(V s) from Hall measurements because $\mu_p = 13 \times 10^{-4}$ m^2/(V s) at room temperature, which is comparable with the carrier mobility in the $CuInGaSe_2$ photovoltaic devices measured using high-frequency admittance studies [19] and $m_n^*/m_p^* = 1.53 \times 10^{-3}$.

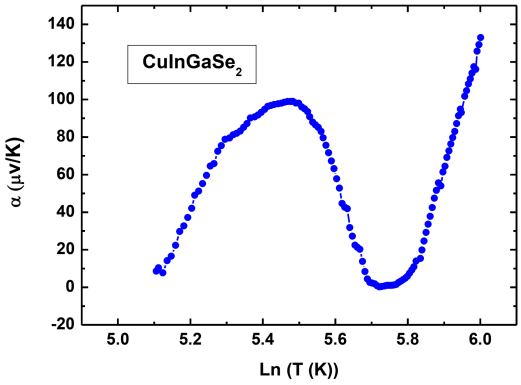

Fig. 3. Relation between thermoelectric power α and $\ln(T)$ for the investigated $CuInGaSe_2$ crystal.

According to the Einstein relation, the diffusion coefficient is stated as follows

$$D = \frac{\mu\, k_{\mathrm{B}} T}{q}, \tag{2}$$

where q is the charge of an electron, k_{B} is the Boltzmann constant, T is the temperature, and μ is the charge carrier mobility.

At room temperature, the diffusion coefficients for majority and minority carriers were calculated and determined to be $D_p = 0.45 \times 10^{-4}$ m^2/s and $D_n = 0.81 \times 10^{-4}$ m^2/s, respectively. These values are in line with what is found in the literature on $Cu_2ZnSnSe_4$ [20].

Wilson [18] proposed another formula to be used in the extrinsic region in order to make better use of the phenomenon

$$\alpha = \frac{k_{\mathrm{B}}}{e}\left[2 - \ln\left(\frac{P h^3}{2\sqrt{\left(2\pi m_p^* k_{\mathrm{B}} T\right)^3}}\right)\right]. \tag{3}$$

In Fig. 3, the relationship (3) between α and $\ln(T)$ is represented. In the impurity region, this relationship reflects a straight-line relationship. As the temperature rises, the thermoelectric power in the impurity zone drops sharply. We get $m_p^* = 7.11 \times 10^{-29}$ kg from the intercept of the line (in the extrinsic range) with the α axis. We can explain why the effective mass of holes is so large. Electron interaction with the lattice, i.e., phonons, results in the effective mass. A hole spends more time in the interaction region as its velocity decreases, implying that holes significantly interact with phonons.

As a result, the effective mass increases. Electron interaction with the lattice, i.e., phonons, results in the effective mass. A hole spends more time in the interaction region as its velocity decreases, implying that holes significantly interact with phonons. As a result, the effective mass increases. When we combine this with the previously mentioned ratio finding, we get $m_n^* = 3.11 \times 10^{-31}$ kg for the minority carrier's effective mass. Because the effective mass values are now available, the relaxation times for both types of carriers can be calculated.

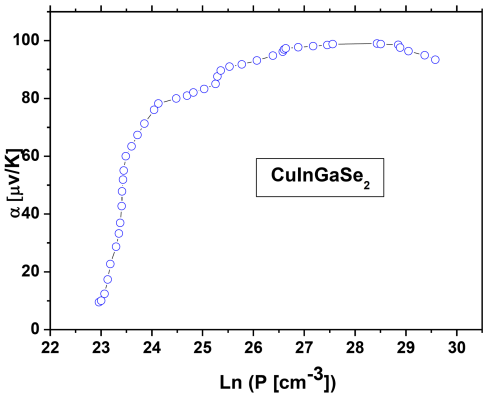

Fig. 4. The characteristics of Seebeck coefficient α and the natural logarithm of the charge carrier concentration in the investigated $CuInGaSe_2$ crystal.

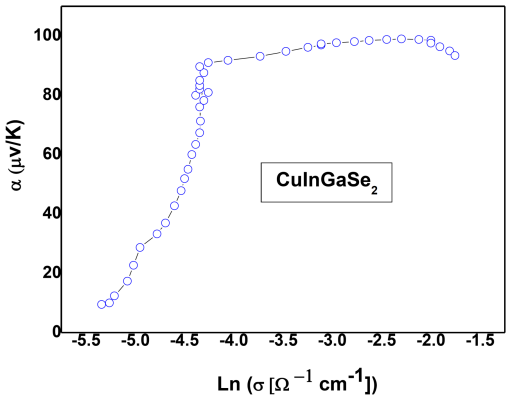

Fig. 5. The characteristics of Seebeck coefficient α and the natural logarithm of electrical conductivity in the investigated $CuInGaSe_2$ crystal.

By using $\tau = \frac{m}{n\rho e^2}$, the predicted relaxation time for holes is 7.18×10^{-4} ps, while the relaxation time for electrons is 4.48×10^{-6} ps.

The diffusion coefficient is inversely proportional to the effective mass of carriers, which makes sense given that the effective mass of holes is greater than that of electrons. Furthermore, the results show that electron mobility is substantially higher than hole mobility, which is acceptable because the effective mass of holes is much bigger than that of electrons.

The average distance travelled by an excited carrier before recombining can be described as the diffusion length of a carrier type in a material. The length of diffusion can be calculated as $L_D = \sqrt{D\tau}$. When the diffusion coefficient and relaxation time are combined, the diffusion length of free charge carriers is $L_p = 0.16$ nm and $L_n = 0.026$ nm for holes and electrons, respectively. The values are consistent with the literature [21]. Heavily doped semiconductor materials have higher recombination rates and, as a result, shorter diffusion lengths. The current study has been expanded to investigate the relationship between α and both the carrier density P and thermoelectric power (in terms of T). Relying on the formula

$$\alpha = \frac{k_B}{e}\left[A + \ln\left(\frac{\sqrt{(2\pi m_p^* k_B T)^3}}{4\pi^3 h^3}\right)\right] - \frac{k_B}{e}\ln(P), \tag{4}$$

we gain a better understanding of the real parameters influencing thermoelectric power (electric conductivity). The dependency of α on the natural logarithm of the charge carrier concentration is shown in Fig. 4. From this trend, we can deduce that the effect of charge carriers is a significant determinant of the fluctuation of α. While we plotting α vs $\ln(\sigma)$ for the $CuInGaSe_2$ sample in Fig. 5, we saw a similar tendency.

The primary conclusion based on Fig. 5 is that the concentration increases at first, and then plateaus abruptly. The following relationship [22] may assist us in comprehending this behaviour

$$\alpha = \frac{k_B}{e}\left[A + \ln\left(\frac{\sqrt{(2\pi\, m_p^* k_B T)^3}}{4\pi^3 h^3}\right)\right] - \frac{k_B}{e}\ln(\sigma). \tag{5}$$

Here, A denotes the normalized constant, i.e., $A = \exp(E_F/(k_B T))$ with the Fermi level E_F and the Boltzmann constant k_B, m_p^* is the effective mass of the hole, and h is the Planck constant. In the temperature range $T < 408$ K, the drop in thermoelectric power with electric conductivity could be due to a decrease in carrier density.

Thermoelectric power (TEP) appears to rise with electric conductivity over 410 K. We may derive from Figs. 4 and 5 that the variation of α with respect to external temperature is not a mobility effect, but rather a concentration effect. The efficiency parameter Z is defined as

$$Z = \alpha^2 \sigma / K, \tag{6}$$

where α, σ, and K are the tested compound's TEP, electrical conductivity, and thermal conductivity ($K = 5$ W/(m K) [23, 24]), respectively, which are used to select materials for thermocouples, thermoelectric generators, and refrigerators.

As a result, the most difficult technological challenge in the development of a successful thermoelectric element is determining how to improve the material's figure of merit (this term refers to a measurement of a thermoelectric element's performance and efficiency). The figure of merit for our $CuInGaSe_2$ samples is $Z = 16.04 \times 10^{-10}$.

The experimental data treatment sheds new light on the major physical parameters of $CuInGaSe_2$ crystals. TEP data revealed pronounced parameters that may be used in practical applications.

The electrical performance of thermoelectric materials is represented in Fig. 6 by the power factor ($PF = \sigma\alpha^2$), which is determined from the data in Fig. 1a and b. As shown in Fig. 6, the power factor PF is nearly unchanged in the temperature range of 186–236 K. As the temperature rises from 237 K,

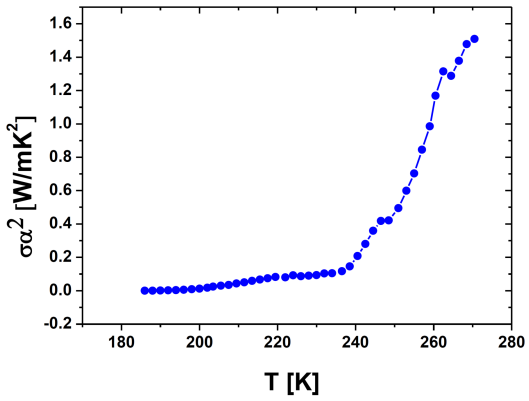

Fig. 6. Temperature dependences of the power factor $\alpha^2\sigma$ for the $CuInGaSe_2$ crystal.

the power factor also increases. The power factor represents a thermoelectric material's ability to generate energy, which increases as the temperature rises.

4. Conclusions

Using the Bridgman–Stockbarger process, a large, centimetre-sized crystal of $CuInGaSe_2$ was successfully produced, allowing for a careful analysis of its thermoelectric power (TEP) over a wide temperature range of 186–424 K. The conductivity of the crystals was identified to be p-type based on these observations. Electron-hole mobility has been discovered. It was calculated what the elective mass of holes and electrons is. The majority and minority carriers' relaxation times were compared. The diffusion coefficient of holes and electrons, as well as their diffusion length, were calculated. The figure of merit was calculated. These studies provide a significant quantity of information regarding actual behaviour as well as the potential for practical application.

References

[1] K. Ahmed, M.S. Tanvir, R. Al Tahmid, M.M. Islam Sagor, M. Ahsanul Haq, M.A. Rahman Swapno, in: *2019 2nd Int. Conf. on Innovation in Engineering and Technology (ICIET)*, 2019, p. 1.

[2] B. Ismail, W. Ahmed, *Recent Pat. Electr. Eng.* **2**, 27 (2009).

[3] B. Ferro, A. Bornschlegell, R. Ramos, in: *XL Ibero-Latin-American Congress on Computational Methods in Engineering*, 2019.

[4] A.M. Dehkordi, M. Zebarjadi, Jian He, T.M. Tritt, *Mater. Sci. Eng. R Rep.* **97**, 1 (2015).

[5] A.M.K.E. Amean, *Int. J. Adv. Res. Plan. Sustain. Dev.* **4**, 69 (2021).

[6] I. Qaiser, T. Grigoriadis, *Asian Dev. Rev.* **37**, 159 (2020).

[7] M.A. Green, A.W.Y. Ho-Baillie, *ACS Energy Lett.* **4**, 1639 (2019).

[8] M. Nakamura, K. Yamaguchi, Y. Kimoto, Y. Yasaki, T. Kato, H. Sugimoto, *IEEE J. Photovolt.* **9**, 1863 (2019).

[9] M. Ochoa, S. Buecheler, A.N. Tiwari, R. Carron, *Energy Environ. Sci.* **13**, 2047 (2020).

[10] Yu-Lun Chueh, *ECS Trans.* **50**, 33 (2013).

[11] S.A. Hussein, A.T. Nagat, *Cryst. Res. Technol.* **24**, 283 (1989).

[12] A.T. Nagat, S.A. Hussein, Y.H. Gameel, A.A. Belal, *Egypt. J. Sol.* **10**, 45 (1988).

[13] A.T. Nagat, S.A. Hussein, Y.H. Gameel, A.A. Belal, *Egypt. J. Sol.* **11**, 60 (1988).

[14] Zilu Liu, in: *Comprehensive Composite Materials II*, 2018.

[15] M.S. Dresselhaus, G. Chen, M.Y. Tang, R. Yang, H. Lee, D. Wang, Z. Ren, J.-P. Fleurial, P. Gogna, *Adv. Mater.* **19**, 1043 (2007).

[16] M. Tufail, W.H. Shah, U. Shah, W.M. Khan, W.A. Syed, A. Safeen, *Chalcogenide Lett.* **16**, 175 (2019).

[17] A. Salem, M.H. Alhossainy, *Mater. Chem. Phys.* **263**, 124436 (2021).

[18] V.A. Johnson, K. Lark-Horovitz, *Phys. Rev.* **92**, 226 (1953).

[19] J.W. Lee, J.D. Cohen, W.N. Shafarman, *Thin Solid Films* **480–481**, 336 (2005).

[20] H. Hempel, C.J. Hages, R. Eichberger, I. Repins, T. Unold, *Sci. Rep.* **8**, 14476 (2018).

[21] A.T. Nagat, S.A. Al-gahtani, F.S. Shokr, S.E. AlGarni, S.R. Al-Harbi K.A. Quhim *Life Sci. J.* **9**, 1495 (2012)

[22] P.H. Schmid, E. Mooser, *Helv. Phys. Acta* **45**, 870 (1972).

[23] D. Sancho-Martínez, M. Schmid, *J. Physics D: Appl. Phys.* **50**, 445501 (2017).

[24] T.J. Silverman, M.G. Deceglie, X. Sun, R.L. Garris, M.A. Alam, C. Deline, S. Kurtz, *IEEE J. Photovol.* **5**, 1742 (2015).